Accounting for Hydroelasticity in the Analysis of Offshore Wind Turbine Spar-Type Platforms

Accounting for Hydroelasticity in the Analysis of Offshore Wind Turbine Spar-Type Platforms

Nikos Mantadakis[1], Eva Loukogeorgaki[1] and Madjid Karimirad[2]
[1]Department of Civil Engineering, Aristotle University of Thessaloniki (AUTh)
Thessaloniki, Greece
[2]Civil Engineering Discipline, School of Natural and Built Environment, Queen's University Belfast
Belfast, United Kingdom

ABSTRACT

In this paper, linear frequency-domain hydroelastic analysis is performed for investigating the behavior of a spar-type supporting platform of a floating offshore wind turbine considering the platform's flexibility. A "dry" mode superposition approach is utilized, where the flexible mode shapes are determined through the application of a FEM based structural model. The diffraction/radiation problem is solved using the boundary integral equation method. Focus is given on the flexible modes' generalized hydrodynamic forcing and responses, the spar's hydroelastic response and the coupling effects between the flexible and the rigid-body modes. For irregular waves, the effect of the peak period on the response spectra and the hydroelastic response is analyzed.

KEY WORDS: Offshore wind turbines; hydroelasticity; supporting structure; spar; mode superposition method; hydroelastic response.

INTRODUCTION

The efficient exploitation of the vast offshore wind energy potential can contribute to the satisfaction of the European Union's energy policy targets in terms of greenhouse gas emissions' reduction, global energy climate change impacts' prevention and energy supply security enhancement. Floating Offshore Wind Turbines (FOWTs) had shown great progress in the past decade facilitating access to deeper waters, where stronger winds exist. In 2017, the world's 1st floating offshore wind farm started its operation (Pineda, 2018), while, currently, extensive investments to build floating offshore wind farms to deeper offshore sites have been decided. To make offshore wind more competitive, offshore wind turbines grew in size. The trend shows a continuous increase in the size of wind turbines (Wind Europe, 2017; Pineda, 2018), which, in turn, requires the utilization of proper, large-size floating supporting platforms for them.

For designing cost-efficient large-size supporting platforms for FOWTs, slender load-carrying structural elements should be engineered to decrease the material used. This fact leads to FOWTs that are characterized by substantial structural deformations, i.e. great flexibility, resulting not only from the tower, but, also from the supporting platform. In these cases, the elastic responses of the supporting platform may become important and the platform's flexibility may affect the dynamic response of the whole floating system. Therefore, the application of an appropriate hydroelastic analysis, accounting for a wave-flexible platform interaction, is very vital towards a reliable and realistic design and structural integrity assessment of this type of structures.

The potential flow theory is normally used to estimate the hydrodynamic forcing and global responses of FOWTs, assuming a rigid body platform. However, recently, several studies have looked at the possibility of including the platform's flexibility, while still using large volume hydrodynamics, in global analyses of FOWTs (e.g. Hegseth et al., 2018). A sectional approach to distribute hydrodynamic loads from linear potential theory over a beam model of the floater may be used (Svendsen, 2016) and a similar method has been proposed by Luan et al. (2017), where sectional loads were derived and compared to the results from a frequency-domain model. On the other hand, Finn (2014) accounted for hydroelasticity in the case of a semi-submersible wind turbine platform, while Kang et al. (2017) performed a time-domain hydroelastic analysis of a multi-unit FOWT.

In the case of spar-type supporting platforms, representing the first commercially deployed floater for FOWTs, Borg et al. (2016) proposed a method, based on the mode superposition approach, for including the platform's flexibility in aero-hydro-servo-elastic simulations. The structural deformations of the spar were described by introducing only one generalized mode (1st in-plane bending mode with shape calculated using a Finite Element structural model), additionally to the six rigid-body modes of the platform. Finally, it is noted that hydroelastic analysis of a slender vertical column based on the mode superposition approach has been implemented by Newman (1994), who utilized orthogonal polynomials (modal functions) to express analytically the flexible mode shapes.

In the present paper, linear hydroelastic analysis is performed for

investigating the behavior of a spar-type FOWT's supporting platform considering its flexibility. The numerical analysis is implemented in the frequency domain and it is based on a "dry" mode superposition approach. In this approach, the generalized (flexible) modes concept is utilized for describing the structural deformations of the platform additionally to the six rigid-body modes, while the required flexible mode shapes are determined in vacuum through the application of a Finite Element Method (FEM) based structural model for solving the corresponding "dry" eigenvalue problem. The diffraction/radiation problem is solved by utilizing the conventional boundary integral equation method. Both regular and irregular waves are considered. For providing additional information on the significance of the flexibility of a spar-type FOWT's platform, focus is given on the generalized hydrodynamic forcing and responses of the flexible modes, on the hydroelastic response of the supporting platform as well as on the coupling effects between the flexible and the rigid-body modes of the examined structure. In the case of irregular waves, the effect of the peak period on the response spectra and the hydroelastic response is also analyzed and demonstrated.

NUMERICAL MODELLING

A catenary moored FOWT with a spar type supporting platform of draft h is placed in an area of finite and constant water depth d (Fig. 1). The tower of the FOWT has a height h_0 above the Mean Water Level (MWL) and a cylindrical cross-section of constant diameter D_0. The spar platform (Fig. 1b) corresponds to a cylinder of constant diameter D_0 and D_1 above and below respectively the taper (conical transition part of height h_2 and of linearly increasing diameter). In order to investigate the hydroelastic behavior of the spar platform, two numerical models are utilized: (a) a 3-D structural model for a "dry" eigenvalue analysis and (b) a 3-D hydrodynamic model for the linear frequency-domain hydroelastic analysis. In the following sub-sections, these two numerical models are described in detail.

3D Structural Model – "Dry" Eigenvalue Analysis

The 3D structural model is based on FEM and it is used in order to conduct a "dry" eigenvalue analysis of the examined floating system. In this way, the "dry" mode shapes of the spar platform are calculated, while, moreover, the generalized structural mass and stiffness matrices (diagonal matrices) are obtained. In the aforementioned structural model, the tower and the spar platform are modeled using shell elements (Karimirad and Moan, 2011), whereas the Rotor-Nacelle-Assembly (RNA) is modeled as point masses at the top of the tower. The mooring lines are taken into account using appropriate springs values.

Considering that the nodal displacement of the structure can be regarded as the superposition of the first N modes and assuming that the free vibration is harmonic with frequency ω^{dry}, the "dry" eigenvalue problem is formed as follows:

$$\left(\mathbf{K}^{\mathbf{str}} - (\omega^{dry})^2 \mathbf{M}^{\mathbf{str}}\right)\mathbf{\Phi} = \{0\} \tag{1}$$

where $\mathbf{\Phi}$ ($6NP$ X N) is the eigenvector matrix, which includes $\boldsymbol{\phi}_\mathbf{j}$ ($6NP$ X 1), j=1,…, N, eigenvectors, $\mathbf{M}^{\mathbf{str}}$ ($6NP$ X $6NP$) and $\mathbf{K}^{\mathbf{str}}$ ($6NP$ X $6NP$) are the structural mass and stiffness matrices, respectively, while NP is the number of nodal points of the mesh of the structural model, including NP^{TWR} nodes for the tower and NP^{SPR} nodes for the spar platform.

The solution of the eigenvalue problem leads to the calculation of the "dry" natural frequency, ω_j^{dry}, for each j^{th}, j=1,…, N, mode, while the corresponding "dry" mode shape $\mathbf{U_j}$ (NP X 3) is formed as follows:

$$\mathbf{U_j} = \left[\mathbf{u_j}\ \mathbf{v_j}\ \mathbf{w_j}\right] = \left[\boldsymbol{\phi}_\mathbf{j}^\mathbf{x}\ \boldsymbol{\phi}_\mathbf{j}^\mathbf{y}\ \boldsymbol{\phi}_\mathbf{j}^\mathbf{z}\right] \tag{2}$$

where $\mathbf{u_j}$ (NP X 1), $\mathbf{v_j}$ (NP X 1) and $\mathbf{w_j}$ (NP X 1) are the component vectors of $\mathbf{U_j}$, while $\boldsymbol{\phi}_\mathbf{j}^\mathbf{x}$, $\boldsymbol{\phi}_\mathbf{j}^\mathbf{y}$ and $\boldsymbol{\phi}_\mathbf{j}^\mathbf{z}$ are sub-matrices of $\boldsymbol{\phi}_\mathbf{j}$ corresponding to the nodal translational degrees of freedom in x, y, z directions respectively. It is noted that eigenmodes for j=1~6 correspond to the six rigid-body modes of the structure, namely, surge, sway, heave, roll, pitch and yaw, whereas eigenmodes for j=7~N present the additional modes (generalized modes) due to flexibility of the tower and the spar.

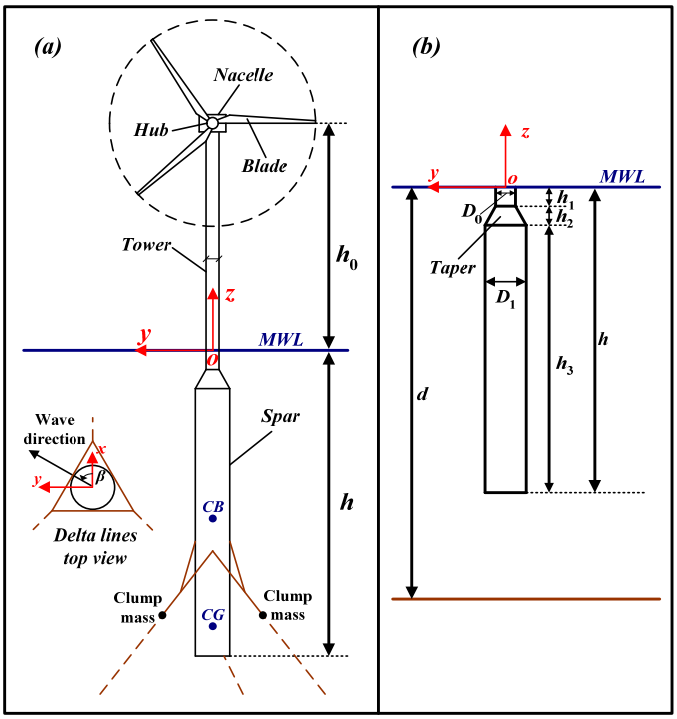

Fig. 1 (a) Schematic layout of the FOWT (from Karimirad and Moan, 2012 with some modifications) and (b) Geometry of the spar platform

In Eq. 1, $\mathbf{M}^{\mathbf{str}}$ and $\mathbf{K}^{\mathbf{str}}$ are positive semi-definite matrices, for which the orthogonally conditions hold, namely:

$$\begin{cases} \left(\boldsymbol{\phi}_\mathbf{j}\right)^\mathrm{T} \mathbf{M}^{\mathbf{str}} \boldsymbol{\phi}_\mathbf{i} = M_{ji}\delta_{ji} \\ \left(\boldsymbol{\phi}_\mathbf{j}\right)^\mathrm{T} \mathbf{K}^{\mathbf{str}} \boldsymbol{\phi}_\mathbf{i} = K_{ji}\delta_{ji} \end{cases} \tag{3}$$

In Eq. 3, M_{ji} and K_{ji} are the generalized mass and structural stiffness coefficients of the j^{th} mode, j=1,…, N, and δ_{ji} is the Kronecker delta. M_{ji} and K_{ji}, i=j=1,…, N, present the elements of the diagonal generalized structural mass ($\mathbf{M}$) and stiffness ($\mathbf{K}$) matrices of N X N dimensions.

Finally, it is mentioned that in the 3D hydrodynamic model only the wetted surface of the FOWT (spar platform) is being modelled using LP panels and, thus, the part of the mode shapes that corresponds to the spar platform should be only taken into account in the corresponding analysis. For calculating the "dry" mode shape for each j^{th}, j=7,…, N, mode at the centers of the LP panels an appropriate interpolation technique is applied, based on the values of $\mathbf{U_j}$, j=7,…, N (Eq. 2) that correspond to the NP^{SPR} nodes of the mesh of the structural model. In this way, the "dry" mode shape for the 3D hydrodynamic model, $\mathbf{U_j^h}$ (LP X 3), for each j^{th}, j=7,…, N, mode is formed (Eq. 4):

$$\mathbf{U_j^h} = \left[\mathbf{u_j^h}\ \mathbf{v_j^h}\ \mathbf{w_j^h}\right] \tag{4}$$

where $\mathbf{u_j^h}$ (LP X 1), $\mathbf{v_j^h}$ (LP X 1) and $\mathbf{w_j^h}$ (LP X 1) are the component vectors of $\mathbf{U_j^h}$, j=7,…, N, in x, y, z directions respectively.

3D Hydrodynamic Model – Hydroelastic Analysis

The hydroelastic analysis of the spar platform under the action of regular waves is implemented in the frequency domain and it is based on a 3D linear wave diffraction theory. In this linear analysis, the platform is assumed to undergo small oscillations of amplitude ξ_j, j=1,…, 6, in all six Degrees of Freedom (DOF) corresponding to the rigid-body modes. Moreover, the (N-6) additional modes of the spar resulting from its structural deformations are expressed as generalized (flexible) modes of body motion with amplitude ξ_j, j=7,…, N.

The fluid is assumed inviscid and incompressible with irrotational motion. Consequently, the fluid motion is described in terms of the velocity potential, satisfying the Laplace equation. Its complex spatial part is defined as (Lee, 1995; Lee and Newman, 2004):

$$\varphi = \varphi_D + i\omega \sum_{j=1}^{N} \xi_j \varphi_j = \varphi_0 + \varphi_S + i\omega \sum_{j=1}^{N} \xi_j \varphi_j \tag{5}$$

where

$$\varphi_0 = \frac{igA}{\omega} \frac{\cosh\left[k(z+d)\right]}{\cosh(kd)} e^{-ik(x\cos\beta + y\sin\beta)} \tag{6}$$

In the above equations, φ_0, φ_S, φ_D and φ_j, j=1,…, N, are the incident, scattered, diffracted and radiation potentials respectively, A and ω are the incident wave amplitude and frequency respectively, β is the incident wave direction (Fig. 1a), g is the gravitational acceleration and k is the wave number.

The solution of the 1st order boundary value problem is based on a 3D dimensional panel method, utilizing Green's theorem and imposing the appropriate boundary conditions on the free surface, the sea bottom, and on the floating body (Lee, 1995; Newman, 1994; Lee and Newman, 2004). The radiation potential, φ_j, for j=7,…, N, is subjected to the following boundary condition on the body boundary (Newman, 1994):

$$\frac{\partial \varphi_j}{\partial n} = n_j = \mathbf{U_j^h} \cdot \mathbf{n} \tag{7}$$

where $\mathbf{n}$=(n_x, n_y, n_z) is the unit normal vector.

Having solved the boundary value problem, the generalized exciting forces, F_i, i=1,…, N, and the generalized added mass and damping coefficients, A_{ij}, B_{ij}, i, j=1,…, N, are calculated as follows:

$$F_i = -i\omega\rho \iint_{S_B} n_i \varphi_D dS \tag{8}$$

$$A_{ij} - \frac{i}{\omega} B_{ij} = \rho \iint_{S_B} n_i \varphi_j dS \tag{9}$$

where S_B is the wetted surface of the spar and ρ is the seawater density.

The amplitudes of the body's motions ξ_j, j=1,…, N, representing the participation of each mode in the forced vibration of the system, are obtained from the solution of the following linear system of equations:

$$\sum_{j=1}^{N} \left[-\omega^2 (M_{ij} + A_{ij}) + i\omega B_{ij} + (C_{ij} + K_{ij} + K_{ij}^{\mathrm{m}}) \right] \xi_j = F_i \quad i = 1,..., N \tag{10}$$

In Eq. 10, M_{ij} and K_{ij}, i, j=1,…, N, present the coefficients of the diagonal generalized structural mass (**M**) and stiffness (**K**) matrices respectively, obtained from the 3D structural model, as mentioned above, while K_{ij}^m are the stiffness coefficients due to the applied mooring system. Moreover, C_{ij} are the generalized restoring-force coefficients, which for i=j=7,…, N are calculated according to Newman (1994).

The generalized response of the spar platform in each mode is expressed in terms of the Response Amplitude Operator (Eq. 11):

$$RAO_j = \frac{|\xi_j|}{A} \qquad j = 1,..., N \tag{11}$$

where $|\xi_j|$ is the amplitude of the complex quantity ξ_j.

On the other hand, the hydroelastic response of the spar, $\mathbf{U_F^{np}} = [u_F^{np}\ v_F^{np}\ w_F^{np}]$, at every np^{th} node, np=1,…, NP^{SPR}, of the spar in the mesh of the structural model is calculated according to the following equations:

$$\left(\mathbf{U_F^{np}}\right)^{\mathrm{T}} = \begin{bmatrix} u_F^{np} \\ v_F^{np} \\ w_F^{np} \end{bmatrix} = \begin{bmatrix} \sqrt{(u_{Freal}^{np})^2 + (u_{Fimag}^{np})^2} \\ \sqrt{(v_{Freal}^{np})^2 + (v_{Fimag}^{np})^2} \\ \sqrt{(w_{Freal}^{np})^2 + (w_{Fimag}^{np})^2} \end{bmatrix} \tag{12}$$

$$\mathbf{U_{Freal}^{np}} = \left[u_{Freal}^{np}\ v_{Freal}^{np}\ w_{Freal}^{np} \right] = \sum_{j=1}^{N} \mathbf{U_j^{np}} \frac{(\xi_j)_{real}}{A} \tag{13}$$

$$\mathbf{U_{Fimag}^{np}} = \left[u_{Fimag}^{np}\ v_{Fimag}^{np}\ w_{Fimag}^{np} \right] = \sum_{j=1}^{N} \mathbf{U_j^{np}} \frac{(\xi_j)_{imag}}{A} \tag{14}$$

where $\mathbf{U_{Freal}^{np}}$ and $\mathbf{U_{Fimag}^{np}}$ are vectors including the real and imaginary part of the hydroelastic response respectively at the np^{th} node, $(\xi_j)_{real}$ and $(\xi_j)_{imag}$ are the real and imaginary parts of ξ_j, j=1,…, N, and $\mathbf{U_j^{np}} = [u_j^{np}\ v_j^{np}\ w_j^{np}]$ is a sub-matrix of the "dry" mode shape of the j^{th}, j=1,…, N, mode that corresponds to the np^{th} node. For the rigid modes (j=1,…, 6), $\mathbf{U_j^{np}}$ is calculated from the corresponding equations included in Loukogeorgaki et al. (2012), while for the rest modes (j=7,…, N), the sub-matrix $\mathbf{U_j^{np}}$ is equal to the np^{th}, np=1,…, NP^{SPR}, row vector of $\mathbf{U_j}$ (Eq. 2).

CHARACTERISTICS OF THE PHYSICAL PROBLEM EXAMINED

The numerical models described in the previous section are applied for the case of the spar platform of the 5 MW (Jonkman, 2007) catenary moored FOWT described in Karimirad and Moan (2011), Karimirad and Moan (2012) and Karimirad (2013). The superstructure of the aforementioned FOWT consists of: (a) the RNA of mass equal to 350,000 kg and (b) the tower of height h_0=90 m (Fig. 1a) and of mass equal to 347,460 kg. The cylindrical platform has a total draft h equal to 120 m, while the whole floating system is placed in an area of constant depth d=320 m (Fig. 1). The part of the platform close to the MWL of height h_1=4 m has constant diameter D_0=6.5 m and it is followed by the taper of height h_2=8 m (Fig. 1b). The remaining part of the spar of height h_3=108 m has constant diameter D_1 equal to 9.4 m. The platform is stabilized by deploying ballast and has a total mass of 7,593,000 kg (center of gravity and of buoyancy of the FOWT including RNA, tower and spar with ballast at 78.61 m and 62.0 m respectively below the MWL). The floating system is moored to the sea floor through a catenary mooring system consisting of three mooring lines with a delta configuration (Fig. 1a). The three mooring lines have in-between angle of 120 deg in the horizontal plane and each of them has a clump mass of 34,506 kg. More details about the mooring system can be found in Karimirad and Moan (2011) and Karimirad and Moan (2012), while Table 1 includes the corresponding K_{ij}^m, i=j=1,…, 6, values considered in Eq. 10.

The platform of the examined FOWT is subjected to the action of regular and irregular incident waves of direction β=0 deg (Fig. 1a). In the case of regular waves, 120 wave frequencies are totally examined, with ω varying between 0.1 rad/s and 6 rad/s. On the other hand, for the case of irregular waves, two different sea states are taken into account with significant wave height H_s=5 m and peak period, T_p, equal to 8 s

and 12 s (peak frequency, ω_p, equal to 0.79 rad/s and 0.52 rad/s respectively). The Jonswap spectrum (DNV – GL, 2017) is utilized with non-dimensional peak shape parameter equal to 3.3.

Table 1. Values of stiffness coefficients due to mooring system

K_{11}^m, K_{22}^m (N/m)	41,684
K_{33}^m (N/m)	10,799
K_{44}^m, K_{55}^m (Nm/rad)	557,212,183
K_{66}^m (Nm/rad)	116,000,000

In the present numerical investigation, the first four generalized modes (corresponding to the 1st and 2nd in-plane and out-of-plane bending modes) additionally to the six rigid-body modes are taken into account (i.e. N=10). The shapes of these modes are obtained by applying the 3D structural model described in the previous section. More specifically, the corresponding "dry" eigenvalue analysis is implemented considering additionally to the spar the flexible tower and a point mass at the top of the tower due to the RNA. The part of the normalized mode shapes of the four bending modes, which corresponds to the platform and used in the present hydroelastic analysis is shown in Fig. 2.

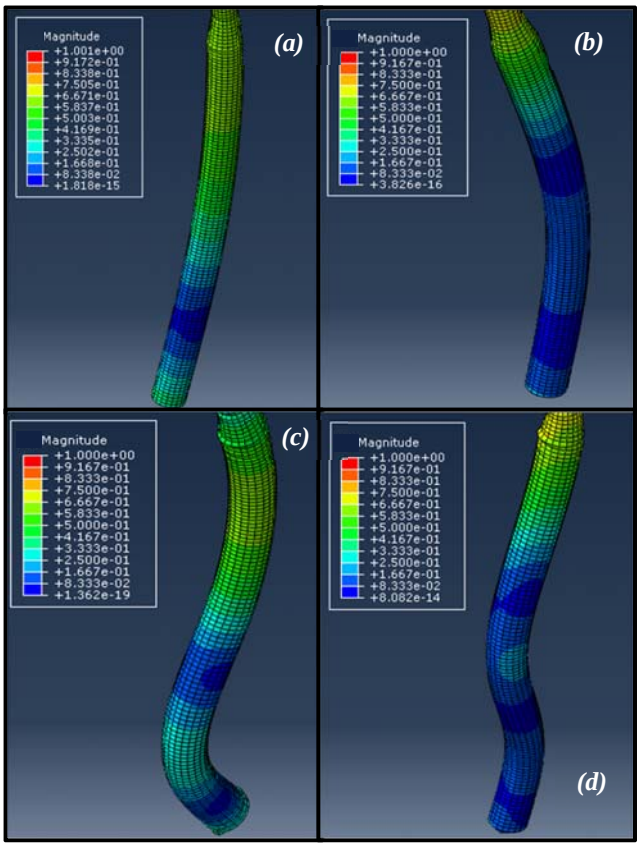

Fig. 2 "Dry" mode shapes of the (a) 1st, (b) 2nd, (c) 3rd and (d) 4th bending modes of the examined FOWT's platform

Finally, it is noted that "wet" natural frequencies, ω_{nj}, j=7~10, for all flexible modes have been calculated taking into account the generalized added mass (Eq. 9) and the generalized restoring-force coefficients, additionally to the generalized mass and structural stiffness. Specifically, ω_{n7} and ω_{n8} have been calculated equal to 1.8005 rad/s and 5.5770 rad/s respectively, while ω_{nj}, j=9 and 10, have values larger than 6 rad/s. As for the rigid-body modes, the natural frequencies ω_{nj}, j=1,…, 6, are equal to 0.0507 rad/s for j=1, 2, 0.2001 rad/s for j=3, 0.3096 rad/s for j=4, 0.3095 rad/s for j=5 and 0.8297 rad/s for j=6.

RESULTS AND DISCUSSION

In the following subsections, the results of the hydroelastic analysis of the examined FOWT's flexible platform are presented and discussed. Focus is given on the generalized hydrodynamic forcing and responses of the flexible modes, on the hydroelastic response of the spar platform, as well as on the coupling effects between the flexible and the rigid-body modes of the examined structure. In the case of irregular waves, the effect of the spectrum peak frequency on the response spectra and the hydroelastic response is presented and discussed. Unless otherwise mentioned, all physical quantities are presented in non-dimensional form, with values obtained using $D_1/2$ as the characteristic length scale for non-dimensionalization.

Exciting Forces and Hydrodynamic Coefficients

Fig. 3 shows the variation of the non-dimensional exciting forces F_i, i=1, 3, 5, 7~10, as a function of ω. F_i, i=1, 5, 7~10, show the same variation pattern characterized by a smooth increase with a maximum value at 0.4 rad/s<ω<1.3 rad/s and a subsequent smooth decrease towards zero values in the examined high-frequency range. F_3 (Fig. 3a) varies in a similar manner; however, contrary to the rest exciting forces, it obtains a local zero value at ω≈0.3 rad/sec. This local minimum is attributed to "counteracting effects" (Tao et al., 2004) resulting from the existence of the taper with the linearly increasing diameter (Fig. 1b). With regard to the generalized exciting forces corresponding to the flexible modes (Fig. 3b), it is worth to note that F_i, i=7~10, have values comparable to the ones of both F_1 and F_3 (Fig. 3a).

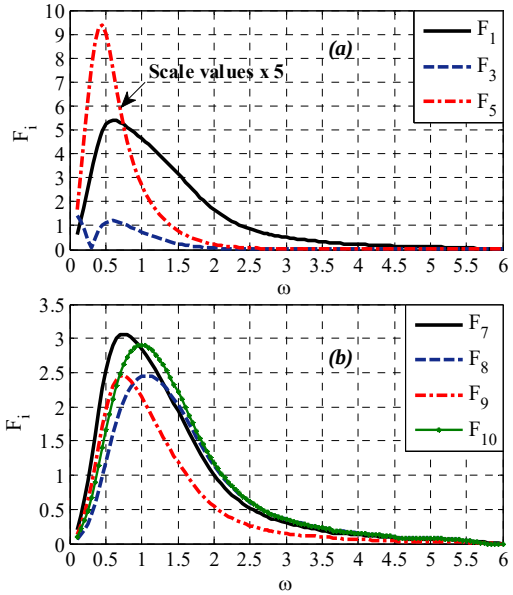

Fig. 3 Variation of F_i, i=1, 3, 5, 7~10, as a function of ω

As for the hydrodynamic coefficients (Figs. 4~5), A_{ij}, i=j=7~10 (Fig. 4c) show a smooth variation in the examined frequency range and values comparable with the ones of A_{33} (Fig. 4a). B_{ij}, i=j=7~10 (Fig. 4e) vary similarly to B_{ij}, i=j=1, 3, 5 (Fig. 4d) and have values comparable with the ones of B_{11}. Moreover, the existence of non-zero off-diagonal coefficients A_{ij}, B_{ij}, i=7~10, j=1, 5 (Fig. 5) indicates coupling of the

flexible modes with the surge and pitch rigid-body modes. It is worth to note that B_{ij}, i=7~10, j=1, 5 (Figs. 5c~5d) show a maximum (positive) or a minimum (negative) value at 0.5 rad/s<ω<1.5 rad/s followed by a smooth decrease or increase respectively towards zero values at higher frequencies. Similar behavior has been observed in Borg et al. (2016).

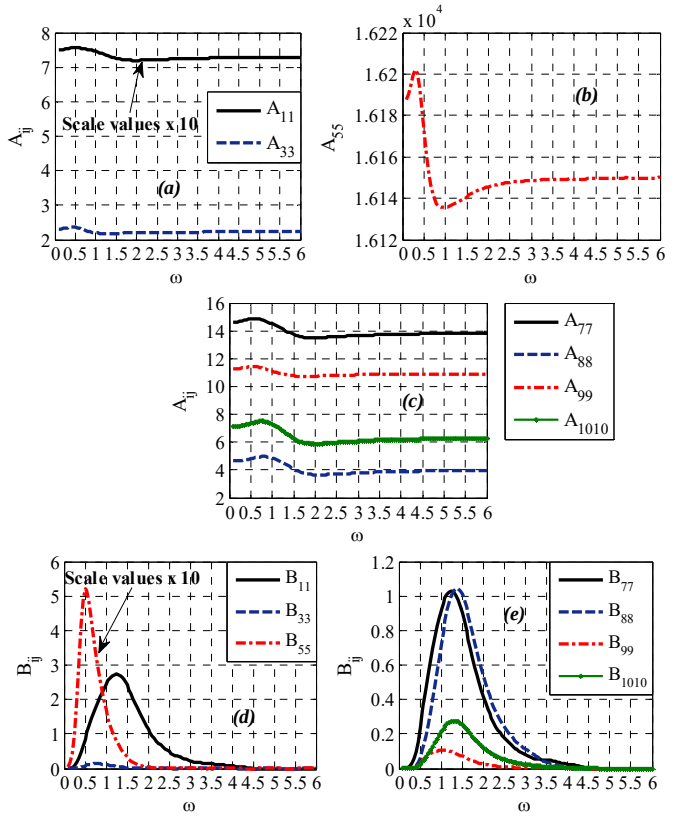

Fig. 4 Variation of A_{ij}, B_{ij}, i=j=1, 3, 5, 7~10, as a function of ω

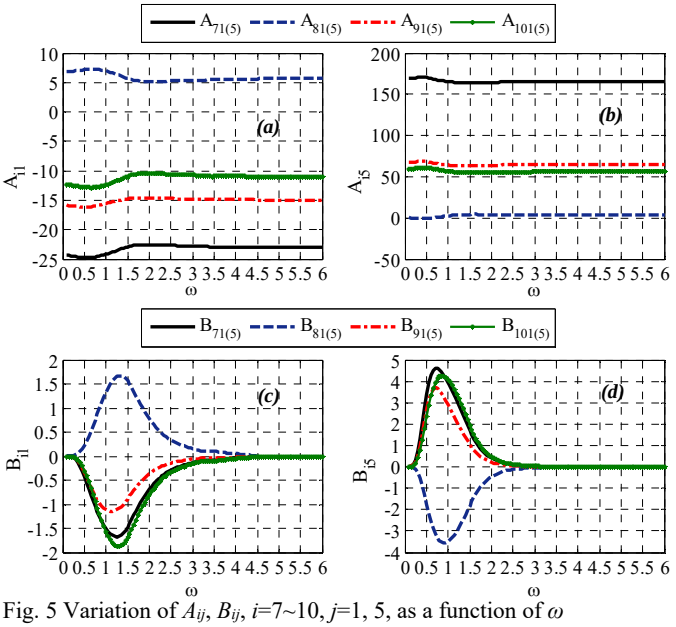

Fig. 5 Variation of A_{ij}, B_{ij}, i=7~10, j=1, 5, as a function of ω

Generalized Response

Fig. 6 shows the variation of RAO_j, j=1, 3, 5, as a function of ω both for the case of the flexible (FLX) platform (solution of Eq. 10 for N=10) and for the case of the rigid (RG) platform (solution of Eq. 10 only for rigid-body modes). Results are presented for 0.1 rad/s≤ω≤2.5 rad/s, where RAO_j, j=1, 3, 5, have significant values. Moreover, in Fig. 6b, the RAO_3 peak values have been truncated for visualization purposes.

In the case of the rigid platform, RAO_1 (Fig. 6a) has a local maximum at ω=0.3 rad/s, attributed to the coupling of surge with pitch and the resonance of the latter DOF (Fig. 6c) at this ω value (ω_{n5}=0.3095 rad/s). RAO_3 (Fig. 6b) show significant values at 0.15 rad/s<ω<0.25 rad/s due to resonance phenomena at this frequency range (ω_{n3}= 0.2001 rad/s). The consideration of a flexible platform has an insignificant effect on RAO_j, j=1, 3, 5, since the values and the variation pattern of the aforementioned quantities are almost the same with the ones obtained in the case of the rigid platform. However, the consideration of the flexible modes of the spar leads to the occurrence of a second local maximum of RAO_j, j=1, 5 (Figs. 6a, 6c) at ω=2.05 rad/s. This fact is attributed to the coupling of surge and pitch with the 7th mode and the existence of a maximum value of RAO_7 at this wave frequency (Fig. 7a).

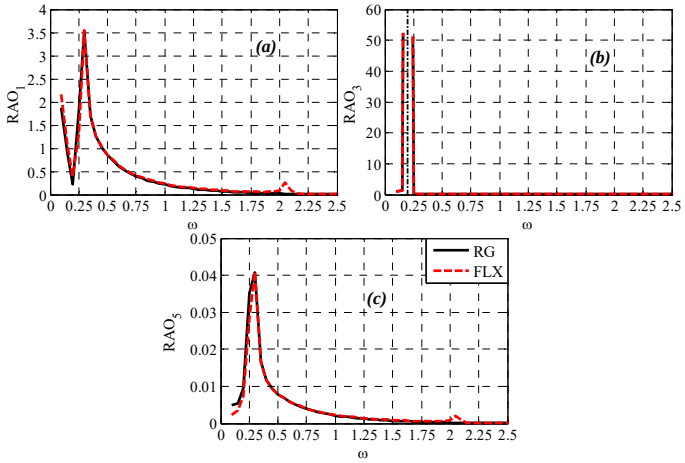

Fig. 6 Variation of RAO_j, j=1, 3, 5, as a function of ω

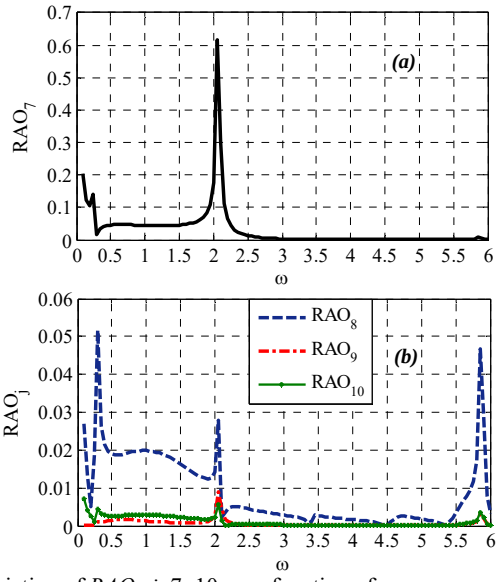

Fig. 7 Variation of RAO_j, j=7~10, as a function of ω

As for RAO_j, j=7~10, of the flexible modes (Fig. 7), RAO_7 (Fig. 7a) shows a smooth variation with a peak value at ω=2.05 rad/s related to the occurrence of resonance (ω_{n7}=1.8005 rad/s). Moreover, a second local maximum is observed at ω=0.25 rad/s attributed to the coupling of the 7th mode with the 1st and 5th rigid-body modes. The variation pattern of RAO_8 (Fig. 7b) is characterized by the existence of: (a) two local peak values at ω=0.30 rad/s and 2.05 rad/s, where RAO_5 (Fig. 6c) and RAO_7 (Fig. 7a) are maximized respectively, due to the coupling of the 8th mode with the 5th and the 7th DOF and (b) a third peak value at ω=5.85 rad/s related to resonance phenomena (ω_{n8}=5.577 rad/s). Finally, RAO_j, j=9~10 (Fig. 7b) are characterized by very small values; therefore, the corresponding mode shapes are not significantly excited in the examined frequency range.

Hydroelastic Response under the Action of Regular Waves

In the case of regular waves, the hydroelastic response of the examined spar has been calculated at ω=0.30 rad/s and ω=2.05 rad/s, where resonance of pitch and of the 7th mode occurs respectively. For these two frequencies, Fig. 8 shows the 3-D deformed shape of the structure, described by $\mathbf{U_F^{np}}$ at all NP^{SPR} nodes of the spar, and the magnitude, $\left|\mathbf{U_F^{np}}\right|$, of $\mathbf{U_F^{np}}$ in all three dimensions and at all NP^{SPR} nodes.

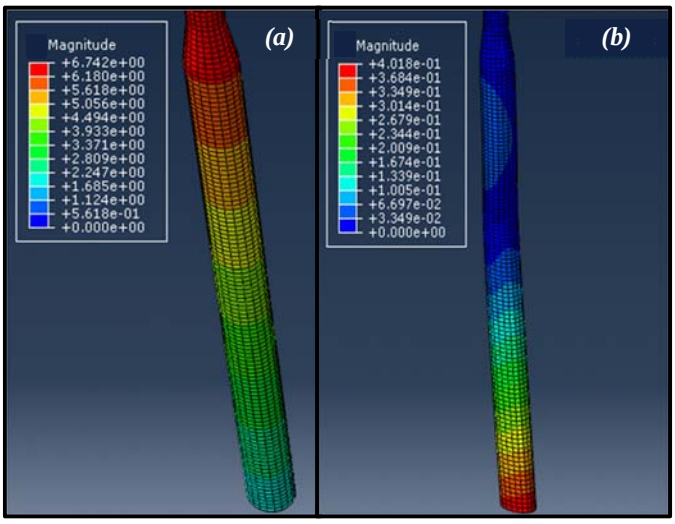

Fig. 8 3-D deformed shapes and contours of $\left|\mathbf{U_F^{np}}\right|$ (m/m) of the spar at: (a) ω=0.30 rad/s and (b) ω=2.05 rad/s

For ω=0.30 rad/s (Fig. 8a), the contribution of the flexible modes of the spar to its hydroelastic response is very small, due to the existence of small RAO_j, j=7~10, values (Fig. 7) and $\mathbf{U_F^{np}}$ is mainly a result of the excitation of the spar's rigid-body modes (especially of pitch and surge). Consequently, $\mathbf{U_F^{np}}$ resembles the response of a rigid body and an almost un-deformed shape of the structure along its length is observed. On the other hand, the significant excitation of the 7th mode at ω=2.05 rad/s (Fig. 7a) leads to a bending-driven deformed shape of the spar (Fig. 8b).

Response Spectra

Considering the action of irregular waves, Figs. 9~10 show the response spectra for rigid-body and flexible modes respectively for two sea states with H_s= 5 m and T_p= 8 s and 12 s described by the Jonswap spectrum. In Fig. 9, results are presented for both the flexible (FLX) and the rigid (RG) platform (solution of Eq. 10 with N=10 and N=6 respectively). It is noted that for a given sea state, the spectral density, $S_{Rj}(\omega \mid H_s, T_p)$, of the response spectrum for each j^{th}, j=1,…, N, mode is calculated using the following equation (e.g. Naess and Moan, 2013):

$$S_{Rj}(\omega \mid H_s, T_p) = \left(RAO_j\right)^2 S(\omega \mid H_s, T_p) \quad (15)$$

where $S(\omega \mid H_s, T_p)$ is the spectral density of the examined incident wave spectrum, while the symbol "|" is used in order to denote given values of H_s and T_p. Moreover, the results of Figs. 9~10 correspond to 0.1 rad/s≤ω≤2.5 rad/s, where S_{Rj}, j=1,…, N, have significant energy content.

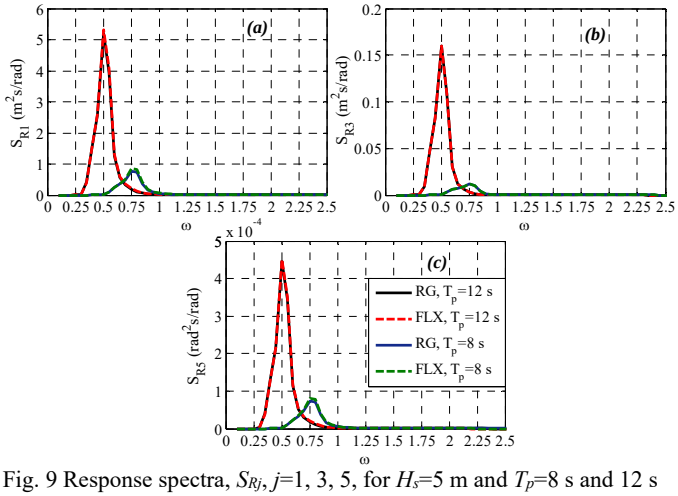

Fig. 9 Response spectra, S_{Rj}, j=1, 3, 5, for H_s=5 m and T_p=8 s and 12 s

With regard to the rigid-body modes (Fig. 9), the consideration of a flexible platform has an insignificant effect on S_{Rj}, j=1, 3, 5, since the corresponding response spectra have the same energy content with the ones obtained in the case of the rigid platform. For both FLX and RG cases, the increase of T_p leads to larger S_{Rj}, j=1, 3, 5, peak values, attributed to the shift of the spectrum peak frequency closer to the frequency range, where resonance of the rigid-body modes occurs.
As for the flexible modes (Fig. 10), the response spectra of the 7th (Fig. 10a) and the 8th (Fig. 10b) mode can be considered to have significant energy content, while the opposite holds true for the 9th and 10th modes (Fig. 10c). In the case of T_p=8 s, S_{R7} (Fig. 10a) is characterized by the existence of two successive peak values; the first one is observed close to ω=ω_p=0.79 rad/s, while the second one at ω=2.05 rad/s, as a result of resonance phenomena. The same variation pattern is also observed for T_p=12 s; however, for this sea state the first peak of S_{R7} occurs at a smaller ω value (close to ω_p=0.52 rad/s), while the energy content of the S_{R7} peak at ω=2.05 rad/s is reduced compared to the case of T_p=8 s. On the other hand, for a given sea state the variation pattern of S_{R8} (Fig. 10b) is characterized by adequate energy content in accordance with the incident wave spectrum.

Hydroelastic Response under the Action of Irregular Waves

Fig. 11 shows the 3-D deformed shape of the examined spar for the two examined sea states. In the case of irregular waves, $\mathbf{U_F^{np}}$ at each np=1,…, NP^{SPR} node of the spar has been calculated by summing up the products of $\mathbf{U_j^{np}}$, j=1, 3, 5, 7~10, with the Root Mean Square (RMS) value of the j^{th} mode's response obtained from the corresponding response spectra (Figs. 9~10).

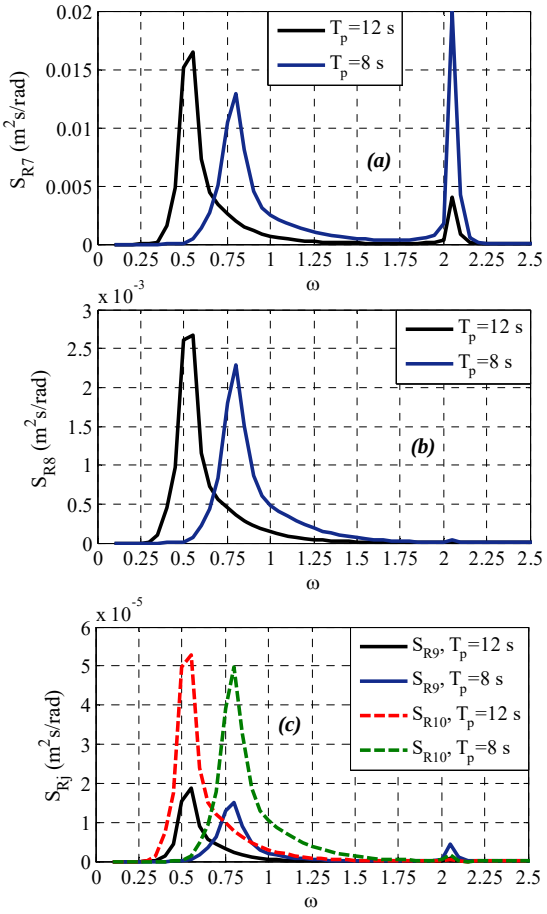

Fig. 10 Response spectra, S_{Rj}, j=7~10, for H_s=5 m and T_p=8 s and 12 s

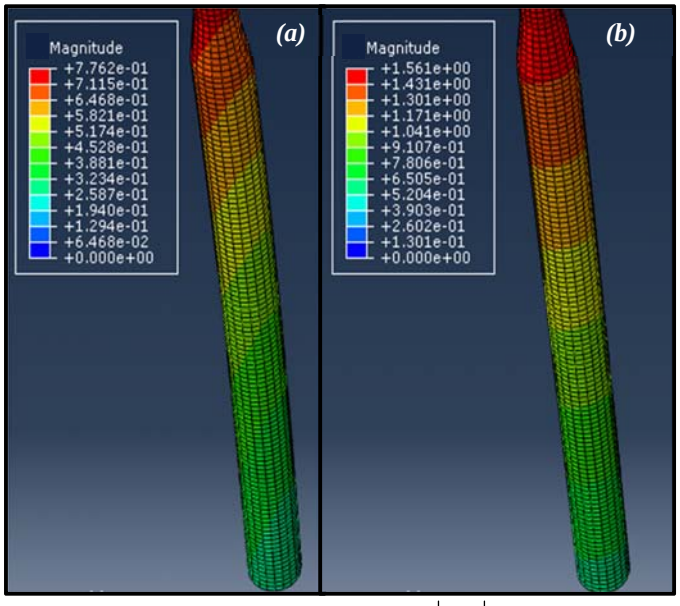

Fig. 11 3-D deformed shapes and contours of $\left|\mathbf{U}_{\mathbf{F}}^{\mathbf{np}}\right|$ (m) of the spar for H_s=5 m and: (a) T_p=8 s, (b) T_p=12 s

In the case of T_p=8 s (Fig. 11a), the 7th and 8th flexible modes of the spar contribute significantly to its hydroelastic response additionally to the rigid-body modes, due to the high energy content of the corresponding response spectra (Fig. 10). Consequently, the deformed shape of the spar is characterized by the existence of bending features. On the other hand, due to the significant energy content of S_{Rj}, j=1, 3, 5, for T_p = 12 s (Fig. 9), an almost un-deformed shape of the spar along its length for this sea state is observed (Fig. 11b) with $\mathbf{U}_{\mathbf{F}}^{\mathbf{np}}$ resembling the response of a rigid body.

CONCLUSIONS

In the present paper, linear hydroelastic analysis is performed in the frequency domain for investigating the behavior of a spar-type FOWT's supporting platform considering its flexibility. The analysis is based on a "dry" mode superposition approach, while the conventional boundary integral equation method is utilized for solving the diffraction/radiation problem. The action of both regular and irregular waves is taken into account. The main conclusions of this study are as follows:

- The generalized exciting forces of the flexible modes of the spar vary smoothly and have values comparable to those of the surge and heave exciting forces.
- The flexible modes are hydrodynamically coupled with the surge and pitch modes through non-zero off-diagonal added mass and radiation damping terms.
- The resonance of the 7th mode has a direct effect on the variation pattern of the generalized response of surge and pitch. This effect is realized through the existence of a second local maximum of RAO_j, j=1, 5, at the frequency range where the aforementioned resonance occurs.
- For the spar platform examined in the present paper, the first two bending modes are significantly excited. Under the action of regular waves, RAO_7 and RAO_8 depict peak values attributed to either resonance or coupling effects with rigid-body modes. In the case of irregular waves, the response spectra of the 7th mode shows a significant energy content at frequencies higher than the examined ω_p, due to resonance of the aforementioned mode.
- Under the action of regular waves, an almost un-deformed shape of the examined FOWT's platform along its length is observed for ω=0.30 rad/s due to the existence of small RAO_j, j=7~10, values. This is not observed for the case of ω=2.05 rad/s, where the significant excitation of the 7th mode leads to a bending-driven deformed shape of the spar.
- In the case of irregular waves, the peak period has a significant effect on the hydroelastic response of the spar. For T_p=8 s the deformed shape of the spar is characterized by bending features, since the response spectra of the 7th and 8th modes have energy content comparable to the corresponding content of the rigid-body modes' response spectra. However, by increasing T_p the contribution of the flexible modes to the hydroelastic response is reduced leading to an almost un-deformed shape of the platform along its length.

The results of the present study illustrate that the elastic responses of a spar-type supporting platform may become important over specific wave frequencies depending upon the incident wave characteristics and the intrinsic dynamic features of the platform. By increasing the wind turbine's size, these responses may be even more significant. Therefore, the inclusion of a flexible spar in coupled/integrated aero-hydro-servo-elastic time-domain stochastic simulations of the FOWT subjected to both wave and wind, will enhance the reliable and robust design of this kind of FOWTs.

REFERENCES

Borg, M, Hansen, AM, and Bredmose, H (2016). "Floating Substructure Flexibility of Large-volume 10MW Offshore Wind Turbine Platforms in Dynamic Calculations," *J Physics: Conference*

Series, 753(8), 082024, DOI: 10.1088/1742-6596/753/8/082024.
Det Norske Veritas – Germanischer Lloyds (DNV – GL) (2017). *Environmental Conditions and Environmental Loads*, Recommended Practice DNVGL-RP-C205, 259.
Finn, T (2014). *Hydroelasticity of a Floating Wind Turbine Platform*, MSc Thesis, Department of Naval Architecture, Kth Royal Institute of Technology, 75.
Hegseth, JM, Bachynski EE, and Karimirad, M (2018). "Comparison and Validation of Hydrodynamic Load Models for a Semi-Submersible Floating Wind Turbine," *Proc ASME 2018 37th Int Conf Ocean*, Offshore and Arctic Eng, Madrid, OMAE2018-77676.
Jonkman, JM (2007). *Dynamics Modeling and Loads Analysis of an Offshore Floating Wind Turbine*, Technical Report No. NREL/TP-500-41958, NREL, 233.
Kang, HY, Kim MH, Kim KH, and Hong, KY (2017). "Hydroelastic Analysis of Multi-unit Floating Offshore Wind Turbine Platform (MUFOWT)," *Proc 27th Int Offshore and Polar Eng Conf*, San Francisco, ISOPE, 1, 554–560.
Karimirad, M, and Moan, T (2011). "Extreme Dynamic Structural Response Analysis of Catenary Moored Spar Wind Turbine in Harsh Environmental Conditions," *J Offshore Mech and Arctic Eng*, ASME, 133(4), 041103-1, doi:10.1115/1.4003393.
Karimirad, M, and Moan, T (2012). "Wave- and Wind-Induced Dynamic Response of a Spar-Type Offshore Wind Turbine," *J Waterw Port Coast Ocean Eng*, 138(1), 9–20.
Karimirad, M (2013). "Modeling Aspects of a Floating Wind Turbine for Coupled Wave-Wind-Induced Dynamic Analyses," *J Renew Energy*, 53, 299–305.
Lee, CH (1995). *WAMIT Theory Manual*, MIT Report 95-2, Dept of Ocean Eng, MIT.
Lee, CH, and Newman, JN (2004). "Computation of Wave Effects using the Panel Method," in *Numerical Models in Fluid–Structure Interaction*, Editor S. Chakrabarti, WIT Press, 1–41.
Loukogeorgaki, E, Michailides, C, and Angelides, DC (2012). "Hydroelastic Analysis of a Flexible Mat-shaped Floating Breakwater under Oblique Wave Action," *J Fluids Struct*, 31, 103–124.
Luan, C, Gao, Z, and Moan, T (2017). "Development and Verification of a Time-Domain Approach for Determining Forces and Moments in Structural Components of Floaters with an Application to Floating Wind Turbines," *Marine Struc*, 51, 87–109.
Naess, A, and Moan, T (2013). *Stochastic Dynamics of Marine Structures*, Cambridge University Press, 422.
Newman, JN (1994). "Wave Effects on Deformable Bodies," *Appl Ocean Res*, 16(1), 47–59.
Pineda, I (2018). *Offshore Wind in Europe - Key Trends and Statistics 2017*, WindEurope, 37.
Svendsen, KF (2016). *Structural Design and Dynamic Analysis of a Tension Leg Platform Wind Turbine, Considering Elasticity in the Hull*, MSc thesis, Norwegian University of Science and Technology, 250.
Tao, L, Lim, KY, and Thiagarajan, K (2004). "Heave Response of Classic Spar with Variable Geometry," *J Offshore Mech and Arctic Eng*, ASME, 126(1), 90–95.
Wind Europe (2017). *Floating Offshore Wind Vision Statement*, WindEurope, 16.

\Conf-std\Template-Word-MS-2019 (0912-2018)